Quantitative characterization of resistive defects in thick composites using step heating thermography

Adel A. Badghaish[a] and David C. Fleming[*a]
[a] Florida Institute of Technology, Mechanical & Aerospace Department, 150 W. University Blvd, Melbourne, FL USA 32901

ABSTRACT

Inspection of thick composite structures, such as Reinforced Thermosetting Resin (RTR) pipes used in the petroleum industry, using infrared thermography is difficult. This paper investigates the use of step heating thermography to increase the maximum detectable defect depth and describes techniques to quantitatively characterize defect depth and severity in thick composites. A procedure to simultaneously determine defect depth and thermal resistance from the early time surface temperature is described. The procedure is based on fitting the early time surface temperature profile over a defect to a one-dimensional three-layer analytical model. Experimental testing demonstrates the accuracy of the procedure.

Keywords: thermography, step heating, composites, nondestructive inspection, delamination, RTR pipe

1. INTRODUCTION

Reinforced Thermosetting Resin (RTR) pipes are increasingly utilized in the petroleum industry to transport corrosive fluids due to their inherent corrosion resistance. RTR pipes are subject to different types of damage during manufacturing, handling, installation and operation. Damage may propagate in service resulting in serious delamination defects. The success of RTR pipes in performing their intended functions depends on their structural integrity and reliability. Accordingly, damage must be identified during scheduled on-stream inspection using effective nondestructive evaluation techniques.

Previous researchers have demonstrated the capability of pulsed thermography to provide quantitative evaluation of delamination defects in thin composite structures, typical of aerospace applications[1,2]. In thick composite structures, such as RTR pipes, the defect detection capabilities of the pulsed thermography are limited to near surface defects. This paper focuses on investigating the capabilities of step heating thermography as a way of increasing the effective depth of detectable defects. Techniques to quantitatively characterize defect depth and severity in thick composite structures are investigated. For high thermal resistance delaminations, the defect depth can be easily predicted using step heating thermography based on the time at which the increase in the surface temperature over the defect deviates from its early time response assuming that the defect will not allow any thermal waves to pass through it, as demonstrated previously by Gupta and Tuli[3]. However, defect identification is more difficult in case of low resistance defects due to the heat diffusion through the defect which leads to reduction in signal strength. Techniques for defect identification of resistive defects have been explored using pulse heating thermography using various techniques by Sun[4], using a technique based on maximum thermal contrast by Maillet et al,[1] and using an eigenvalue decomposition technique, by Winfree and Zalameda[2]. Similar techniques are needed for defect identification of resistive defects using step heating thermography.

This paper describes a procedure to determine defect depth and thermal resistance from the early time surface temperature profile for step heating thermography using a two-point correlation. Analytical techniques similar to those previously applied by Maillet et al[1] for pulse heating are used to provide results that form the basis for the technique. The procedure is based on fitting the early time surface temperature profile over the center of the defect to a one-dimensional three-layer analytical model. Finite element models are used to explore the range of applicability of the method. Experimental testing is performed to demonstrate the accuracy of the proposed procedure for predicting the defect depth and thermal resistance.

[*] dfleming@fit.edu; phone 1 321 674-7241

Thermosense XXX, edited by Vladimir P. Vavilov, Douglas D. Burleigh,
Proc. of SPIE Vol. 6939, 693916, (2008)
0277-786X/08/$18 · doi: 10.1117/12.777064

2. STEP HEATING THERMOGRAPHY

Step heating thermography is a nondestructive inspection technique that monitors the surface temperature rise of the structure with respect to time during the application of a continuous step heating pulse[5]. A typical experimental setup for step heating thermography consists of a heat source and an infrared imaging system, as shown in Figure 1. The simplicity of the required equipment and testing procedures makes it attractive for field applications. Unlike conventional pulsed thermography, low power heating is used. The evolution of the surface temperature profile as a function of time depends on the heat diffusion inside the structure, which is affected by the existence of embedded defects. For an infinitely thick homogeneous structure, the surface temperature will rise linearly with respect to the square root of time. For a finite thickness structure, this linear temperature rise will be affected by reflections of the thermal wave from the rear surface resulting in nonlinear increases in the temperature response beginning at a time characteristic of the thickness. The presence of internal defects will produce similar variations in the temperature with magnitudes and times characteristic of the defect location and severity. The following sections describe the analysis of step heating thermography and evaluate techniques proposed for quantitative defect identification.

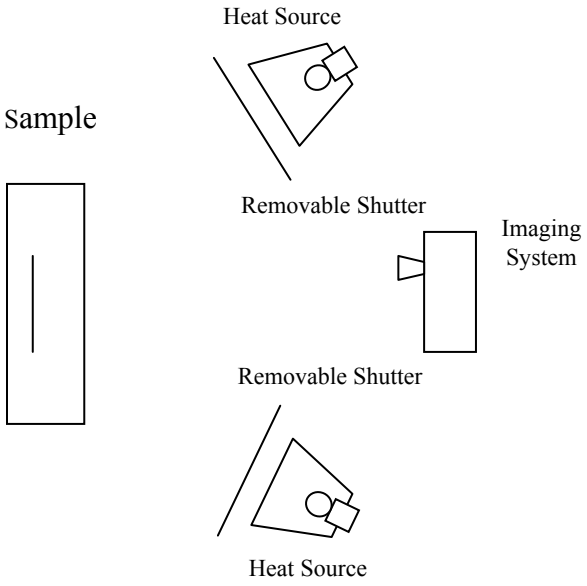

Figure 1. Experimental setup for step heating thermography.

3. ANALYTICAL APPROACH

Analysis of step heating thermography is made using one-dimensional heat transfer models. Subsequent finite element modeling shown in Section 4 demonstrates the applicability of these models provided the defect planar area is sufficiently large compared to the thickness dimensions. Equations of one-dimensional heat conduction in a homogeneous material are well known and described in numerous handbooks such as Carslaw and Jaegar[6]. For example, the surface temperature, T, above plate of infinite thickness (a semi-infinite plate) can be expressed as[6]:

$$T = \frac{2Q}{\kappa}\left(\frac{\alpha t}{\pi}\right)^{\frac{1}{2}}, \tag{1}$$

where Q is the uniform heat flux, κ is the thermal conductivity of the material, and α is the thermal diffusivity. This is the well-know relationship that the temperature varies linearly with the square root of time. For plates of finite thickness under step heating, the surface temperature varies as[6]:

$$T = \frac{2Q}{\kappa}\left(\frac{\alpha t}{\pi}\right)^{\frac{1}{2}}\left[1 + \sqrt{\pi}\sum_{n=1}^{\infty} 2\text{ierfc}\frac{nL}{\sqrt{\alpha t}}\right], \tag{2}$$

where L is the thickness of the plate, and ierfc is the integral of the complementary error function. For small characteristic times, the response is the same as that of a semi-infinite thickness, but as t increases, the response deviates from the semi-infinite plate behavior due to reflections from the back wall.

For inhomogeneous plates or plates containing defects, analytical solutions become more difficult. Maillet et al[1] developed a technique for analyzing one-dimensional heat conduction in layered materials based on the so-called "quadripole method." Maillet et al used this method to study pulsed thermography. In this paper, the approach of Maillet et al is applied for step heating thermography. Figure 2 shows a material containing a defect of infinite extent subject to step heating modeled as a three-layer model.

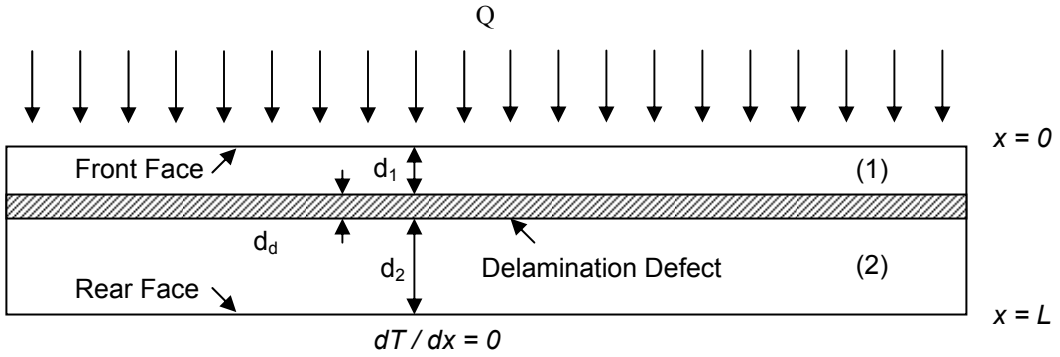

Figure 2. Geometry of the one dimensional model containing finite resistance defect.

In quadripole method, the one-dimensional transient heat transfer in layered structure is modeled by the response through a sequence of homogenous quadripoles, each of which describes heat transfer through a homogeneous medium in terms of temperatures and heat fluxes on the boundaries of the layer. Response within each quadripole is based on well-known one-dimensional heat transfer solutions for homogeneous materials, expressed using Laplace transforms. The Laplace transforms of temperature $\Theta(s)$ and heat flux $\Phi(s)$ of the front and rear surface of the structure are the measures that characterized the response in quadripole method. The following is the response in a single quadripole[1]:

$$\begin{Bmatrix}\Theta_i\\ \Phi_i\end{Bmatrix} = \begin{bmatrix}\cosh(kd) & \left(\sinh(kd)\right)/k\kappa\\ k\kappa\sinh(kd) & \cosh(kd)\end{bmatrix}\begin{Bmatrix}\Theta_o\\ \Phi_o\end{Bmatrix} = \mathbf{M}\begin{Bmatrix}\Theta_o\\ \Phi_o\end{Bmatrix}, \tag{3}$$

where $k = \sqrt{s/\alpha}$, κ is the thermal conductivity, d is the layer thickness, α is the thermal diffusivity, s is the Laplace transform of the time variable and the subscripts i and o refer to the "input" and "output" sides of the layer, respectively. In case of a thin layer which might represent a delamination defect, the matrix **M** can be approximated by

$$\mathbf{M_d} = \begin{bmatrix}1 & R_d\\ 0 & 1\end{bmatrix}, \tag{4}$$

where resistance $R_d = d_d/\kappa$. For a multi-layered structure, the response can be defined by a straightforward matrix multiplication as follows:

$$\begin{Bmatrix}\Theta_f\\ \Phi_f\end{Bmatrix} = \mathbf{M}_1\mathbf{M}_2\mathbf{M}_3\ldots\mathbf{M}_N\begin{Bmatrix}\Theta_r\\ \Phi_r\end{Bmatrix}. \tag{5}$$

where *f* and *r* represent the front and rear surfaces, respectively. In the present problem, there are only three layers, the middle layer is modeled by Equation 4. Solutions for the surface temperatures can be obtained based on the applied heat flux at both surfaces. In step heating, constant heat flux is applied only at the front surface (Φ_f) while adiabatic condition is assumed at rear surface ($\Phi_r = 0$). The applied heat in step heating is represented by $\Phi_f(s) = Q/s$ where Q is the constant applied heat flux. Solutions for the surface temperatures can be obtained easily by matrix multiplication in the Laplace domain. Inversion of the Laplace transform is needed to acquire the surface temperatures in the time domain. Because theoretical inversion of the solutions is prohibitively complicated, a numerical inversion procedure described by Brancik[7] was applied.

For greater generality, the response is presented using nondimensional parameters. A nondimensional time parameter ψ is defined as $\psi = \sqrt{\alpha t}/d_1$, where d_1 is the depth of the defect. Temperature is nondimensionalized as a ratio of a response over the defect area to that of a defect-free semi-infinite plate of same material properties subject to the same heat flux $\overline{T} = T/T_\infty$. A nondimensional resistance ratio is defined as the resistance of the defect to the resistance of the material over the defect, $\overline{R} = R_d/R_{d_1}$. Figure 3 illustrates results for resistive defects with resistance ranging from extremely large (essentially equivalent to a flat-bottom defect) to a resistance of zero (no defect). It can be observed that qualitatively, for all nonzero resistance ratios the nondimensional time at which the temperature ratio deviates from unity is the same, and this "separation time" is therefore characteristic of the depth of the defect. However, for practical application to experimental or field testing it is necessary to establish a rigorous criterion defining "separation time." For example, separation time may be defined as some prescribed deviation of the temperature ratio from unity, such a 1% deviation ($\overline{T}$ =1.01) or 5% deviation ($\overline{T}$ =1.05).[3,8] As seen in Figure 3, the characteristic separation time ψ_s corresponding to 1% or 5% deviation depends on the resistance of the defect.

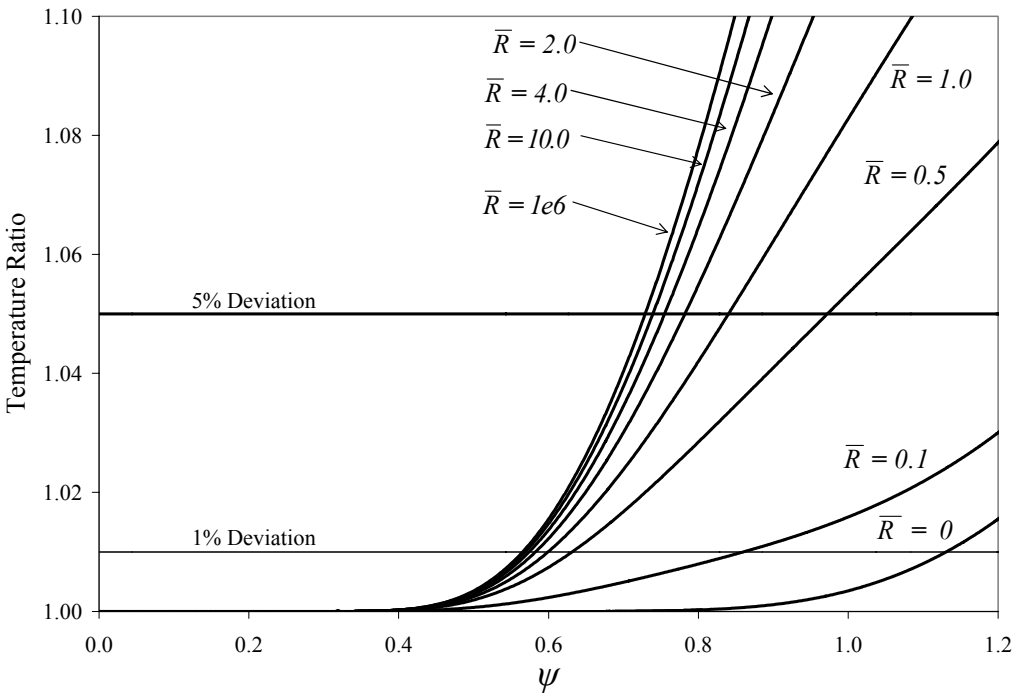

Figure 3. Temperature ratio versus nondimensional time for different resistances.

3.1 Defect depth identification for high resistance defects

For large resistance ratios, (say, above 10), the effect of $\overline{R}$ on ψ_s is small. Many previous studies on defect identification have used the concept of separation time, with the times correlated to an infinite resistance solution to estimate defect

depth.[3,8] This is appropriate for so-called "flat bottom hole" specimens, which are used by previous researchers, often for pulse heating, to characterize loss of wall thickness or to investigate embedded defects by assuming they provide high thermal resistance[3,4,9]. For the present case, the infinite resistance solution results in $\psi_{s,1\%} = 0.5655$ and $\psi_{s,5\%} = 0.7291$, which can be used to estimate defect depth by applying the definition of ψ resulting in:

$$d_1 = \sqrt{\alpha t_{1\%}} \,/ 0.5655 \quad \text{or} \quad d_1 = \sqrt{\alpha t_{5\%}} \,/ 0.7291 , \tag{6}$$

where $t_{1\%}$ and $t_{5\%}$ are experimentally obtained times at which the thermal signal deviates from the semi-infinite solution (which is the initial linear temperature rise with respect to square root of time) by 1% and 5%, respectively. In the absence of the defect or for a defect with no resistance ($\overline{R} = 0$), the separation time is governed by the total thickness of the structure and the thickness can be determined based on infinite resistance ratio results, as shown in Equation 7:

$$L = \sqrt{\alpha t_{1\%}} \,/ 0.5655 \quad \text{or} \quad L = \sqrt{\alpha t_{5\%}} \,/ 0.7291 , \tag{7}$$

where L is the total thickness of the structure.

3.2 Defect depth identification for finite resistance defects

For small resistance ratios the computed separation time is strongly affected by the defect resistance, as seen in Figure 3. Because of heat passing through a low-resistance defect, while separation nominally begins at the same time in all cases, the rate of increase of the temperature ratio is smaller for low resistance ratios altering the measured 1% and 5% separation times. It can also be observed in Figure 3 that at higher percent deviations, the effect of resistance ratio on the measured separation time is greater. Figure 4 illustrates this, by plotting the nondimensional separation time ψ_s as a function of resistance ratio. If the defect resistance is known in advance, then Equation 6 can be corrected by substituting the correct separation time constants, $\psi_{s,}$ from Figure 4 for the constants in Equation 6 (thus correlating with the appropriate one-dimensional resistive model as opposed to the one-dimensional infinite resistance solution). However, it is unreasonable to expect that the defect resistance will be known *a priori* for general defects.

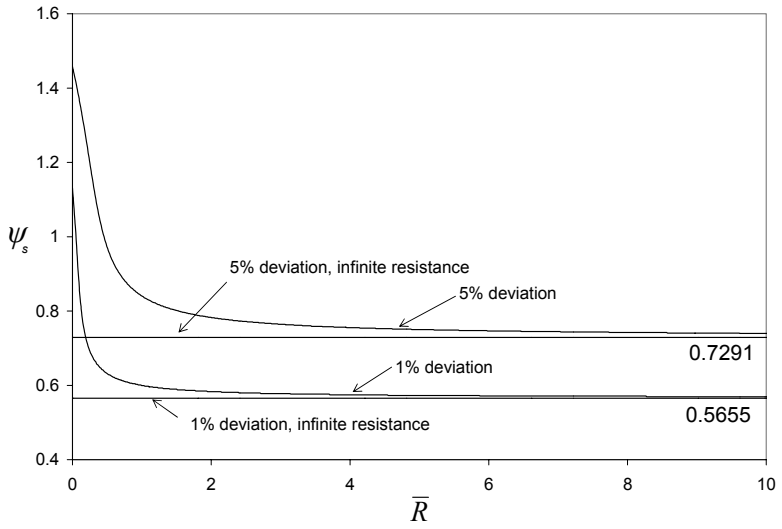

Figure 4. Effect of resistance ratio on computed normalized separation time as predicted by the one-dimensional multi-layer model.

3.3 Simultaneous defect depth and resistance identification for finite resistance defects

While it is well known that a defined separation time can be used to determine defect depth for highly resistive defects through correlation with a one-dimensional analytical solution, and it is shown above that such procedures can be adapted for finite resistive defects to predict the defect depth provided that the defect resistance is known in advance, a more general procedure is needed to simultaneously determine both an unknown defect depth and defect resistance. As observed in Figure 3, the nature deviation of the temperature from unity depends on both the defect depth and the resistance. For any unique combination of two separation times (for example, based on 1% and 5% separation times) there is a unique combination of defect resistance and depth that provides that thermal signature. This provides the basis

for a so-called two-point method for defect identification, which was briefly introduced in Badghaish and Fleming[8]. Two unique separation times such as the 1% and 5% separation times can be used to uniquely determine the corresponding defect depth and defect thermal resistance. Calculations to apply the two-point method are based on the one-dimensional multilayer solution described above. To simplify the following presentation, parameters are nondimensionalized differently from Section 3.2. Now, nondimensional parameters are defined based on the total thickness of the part L, rather than the defect depth d_1:

$$t^* = \frac{\alpha}{L^2}t; \quad X^* = \frac{d_1}{L}; \quad R^* = \frac{R_d}{R} = \frac{\frac{d_1}{\kappa_d}}{\frac{L}{\kappa_c}}, \tag{8}$$

where κ_c is the thermal conductivity of the composite material, which is assumed uniform through the thickness. Using the one-dimensonal solution, contours of equal $\sqrt{t^*_{1\%}}$ and $\sqrt{t^*_{5\%}}$ can be plotted as functions of the defect depth parameter X^* and the defect resistance parameter R^*. This is shown in Figure 5(a), from Badghaish and Fleming[8]. As can be seen, for each pair of separation times, there is one unique intersection between the contours. This is illustrated in Figure 5(b), which shows contours corresponding to nondimensional separation times $t^*_{1\%} = 0.0863$ and $t^*_{5\%} = 0.1644$, and the resulting determination of the nondimensional depth and resistance ratios, from which the defect depth and resistance can be determined. Procedures to compute the one-dimensional multilayer solution and to calculate defect depths and resistance using the two-point method were implemented in MATLAB, and can be easily applied to experimental data. The only inputs required are the separation times and the nominal full thickness of the material, L.

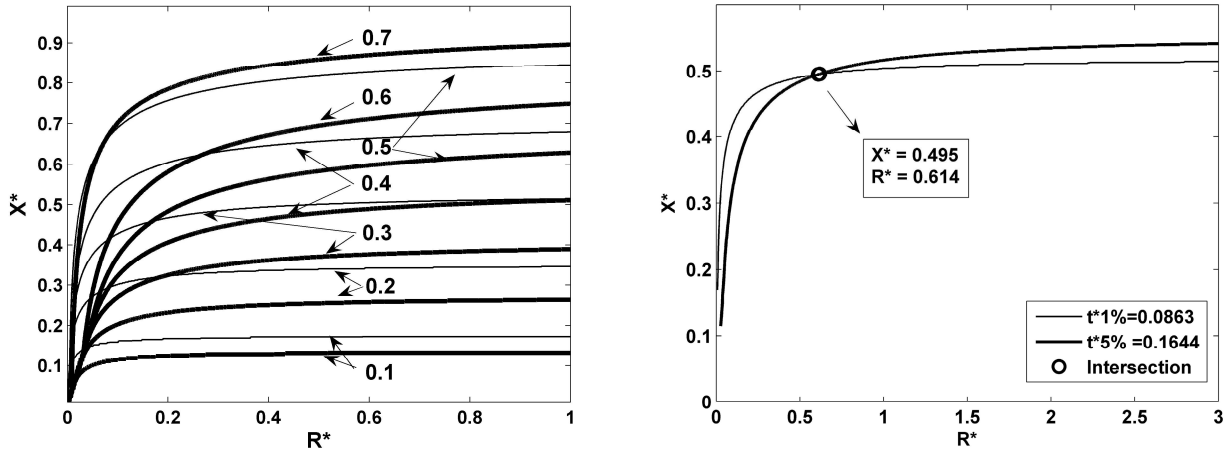

(a) (b)

Figure 5. Demonstration of two-point method: (a) contours of equal square root of nondimensional separation time (thin lines, 1% deviation, thick lines, 5% deviation), from Reference 8. (b) Intersection of contours for a particular pair of separation times leading to calculation of depth and resistance ratios.

4. FINITE ELEMENT MODELING

Because the methods described in Section 3 are based on one-dimensional heat transfer solutions, it is important to understand their limitations with respect to three-dimensional effects. It has been formerly observed in pulsed thermography[9] and stepped heating thermography[3] that the early time behavior of the temperature rise over the center of the defect depends on the defect depth and is independent of the lateral defect size for large defects. Maillet et al.[1] concluded that errors in pulsed thermography due to three-dimensional defect geometry are small if the defect diameter is four times larger than the slab thickness. Lau et al.[10] analyzed the response of defects of different diameters located at same depth using pulsed thermography and found that the early time behavior of all cases closely followed the one-

dimensional result. Because two- or three-dimensional solutions are prohibitively complicated, finite element simulations were used to address this issue for the case of step heating. Test geometries appropriate for the present study were used. Axisymmetric models of heat transfer were conducted using ANSYS Version 10 to demonstrate limitations of the one-dimensional model in three-dimensional cases and for comparison with experimental test results. Similar models are described in Badghaish and Fleming[8]. Results here focus on the case of embedded defects with finite resistance. Defects were simulated as disk-shape inclusions, as shown in Figure 6(a), corresponding to the test geometry used in the experiments. Thermal resistance of the defect was varied by modifying the defect thickness and/or its thermal properties. All simulations were performed using material properties for Glass Fiber Reinforced Plastic (GFRP) specimens containing air filled disk-shaped inclusions, with material thermophysical properties listed in Table 1[5,11].

The models were meshed with four node quadrilateral elements (Plane 55). The element edge length over the defect and through the specimen thickness was 0.1 mm and a more refined mesh with 0.025 mm element edge length was selected through the defect thickness, while the rest of the model was mapped meshed using 25 divisions with a spacing ratio of 2, as shown in Figure 6(b). A time step of 0.1 second was selected based on parametric study. Finite element analyses were performed in a GFRP sample with defect depth d_1 = 2.0 mm and resistance ratio $\overline{R}$ = 1.12. Defect size ratio $\overline{b}$ (the ratio of the defect radius to the defect depth) was varied from 1 to 12. All models had 30 mm radius and 4 mm thickness. Figure 7 illustrates the temperatures rise over the center of the defects with respect to the square root of time and Table 2 compares results for these models.

Table 1. Material thermophysical properties.[5,11]

Material	Density (kg/m^3)	Specific Heat (J/kg-K)	Thermal Conductivity (W/m-K)
GFRP	1770	1200	0.58
Defect	1.2	1006	Varies

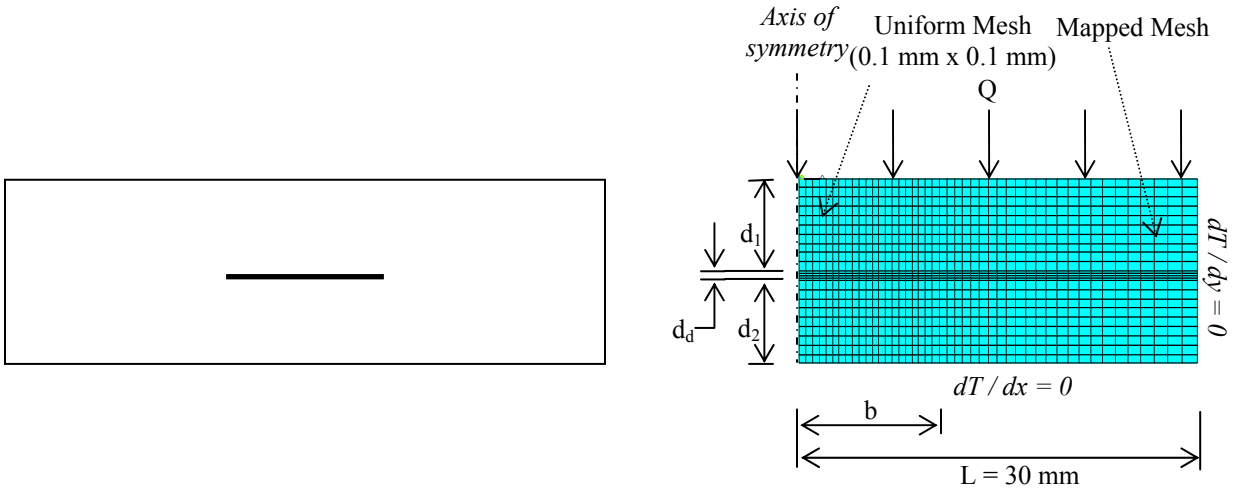

Figure 6. (a) Geometry of specimen containing disk-shaped inclusion, (b) Typical mesh of specimen containing disk-shaped inclusion.

Figure 7 shows that the results are equivalent for this case provided the defect size ratio was greater than approximately four. More detailed results in Table 2 show that the effects of the finite size are more pronounced at greater times. For example, the computed separation times based on 1% deviation were consistent for all defect size ratios greater than 2. For the 5% separation time criterion, consistent results were achieved at ratios from 4 and above. These results are consistent with previous research for step heating discussed above.

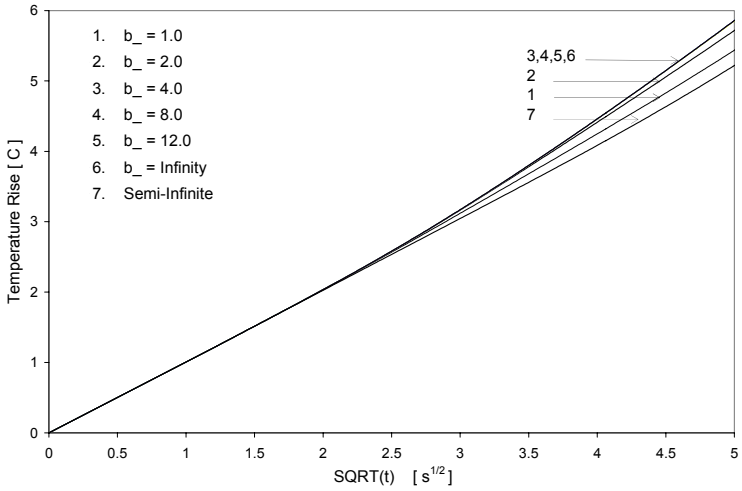

Figure 7. Temperature rise over defects with different sizes.

Finite element results are also used to illustrate the defect identification methods described in Section 3. Defects with different depths, but equal defect resistance ratio ($\overline{R}$ =1.115) and defect size ratio ($\overline{b}$ = 4.0) were modeled, and the resulting surface temperature calculations were used to "predict" the defect depths and resistances. The dimensions of the defects have been adjusted to maintain the same defect resistance and size ratios as the defect depth increases. All models have a total radius of 30 mm, and a 10 mm thickness. Uniform continuous heat flux of magnitude 1 kW/m^2 was prescribed for the top surface while adiabatic conditions were considered for all other surfaces. For the infinite resistance approximation of Section 3.1, Equation 6 was used to calculate defect depth. Because the resistance ratio is known, the finite resistance approach of Section 3.2 can be used to obtain more accurate depth prediction. For this case, the modified equation for these cases will be as follows:

$$d_1 = \sqrt{\alpha t_{1\%}} \,/ 0.5964 \quad \text{or} \quad d_1 = \sqrt{\alpha t_{5\%}} \,/ 0.8282 \,. \tag{9}$$

For the two-point method described in Section 3.3, only the total thickness of the part is needed for input. Results of these calculations are presented in Table 3. Results illustrated in Table 3 shows that considerable errors are expected for finite resistance defects when correlation with the infinite resistance solution is used, even for the moderately large resistance ratio used in this example. As expected, errors are greater by this method when using the 5% separation time than for the 1% separation time. The results also show a trend toward increasing error as the depth of the defect increases. Errors due to the finite resistance ratio can be virtually eliminated if the resistance is known in advance, as demonstrated in Table 3 for the finite resistance correlation. Here, all errors are 1.5% or less. The two-point method, utilizing the techniques of Section 3.3, shows good results for predictions of both defect depth and resistance ratio in all cases, except for the resistance ratio of the shallow defect.

Table 2. Effect of defect radius on separation time.

Defect Size Ratio, $\overline{b}$	Defect Resistance (m^2-K/W)	1 % Separation Time (s)	5 % Separation Time (s)
∞	3.85x10^{-3}	5.1	10.1
12.0	3.85x10^{-3}	5.1	10.1
8.0	3.85x10^{-3}	5.1	10.1
4.0	3.85x10^{-3}	5.1	10.1
2.0	3.85x10^{-3}	5.1	10.5
1.0	3.85x10^{-3}	5.7	N/A

N/A: Cannot be computed from available data

Table 3. Defect depth and resistance determination using the infinite resistance correlation, finite resistance correction, and the two-point resistive solution.

Finite Element Model			Infinite Resistance Correlation		Finite Resistance Correlation		Two-Point Method	
Defect Depth, mm	1 % Separation Time, s	5 % Separation Time, s	1% Sep. Predicted Defect Depth, mm (Error, %)	5% Sep. Predicted Defect Depth, mm (Error, %)	1% Sep. Predicted Defect Depth, mm (Error, %)	5% Sep. Predicted Defect Depth, mm (Error, %)	Predicted Defect Depth, mm (Error, %)	Predicted Resistance Ratio, N.D. (Error, %)
2.0	5.08	10.00	2.08 (4.0)	2.27 (13.5)	1.97 (-1.5)	2.00 (0.0)	1.95 (-2.5)	0.97 (-13.0)
4.0	20.66	40.12	4.20 (5.0)	4.54 (13.5)	3.98 (-0.5)	4.00 (0.0)	3.98 (-0.4)	1.09 (-2.7)
6.0	47.45	90.88	6.37 (6.2)	6.83 (13.8)	6.04 (0.7)	6.02 (0.3)	6.04 (0.7)	1.15 (2.7)

5. EXPERIMENTAL INVESTIGATION AND DISCUSSION

Experimental investigation was performed on specimens made from pultruded fiberglass reinforced polyester panels manufactured by Bedford Reinforced Plastics, Inc. Step heating was provided by two 500 Watt halogen lamps. Surface temperatures were monitored using an IR-FlexCam camera. The camera has focal plane array, uncooled microbolometer 160 x 120 detector. It operates at 8 μm to 12 μm spectral band and has a sensitivity of 0.08 °C with accuracy of 2%. The camera and its software have the ability to record images at a rate of 1 Hz.

The behavior of resistive defects was studied using specimens containing resistive defects represented by thin voids of trapped air. In these specimens, two disjoint panels of composite material, one undamaged and one into which circular defects were milled with 50 mm diameter at a depths between 38 μm and 300 μm, were clamped together as shown in Figure 8. All GFRP panels were machined to provide uniform thickness and smooth contact surfaces and hence to minimize resistance across the contact interface. Assumed properties of these materials are shown in Table 1. Figure 9 presents the thermal responses over the center of typical defects, comparing results obtained through the experiment with finite element results. Good agreement between the experimental and finite element results is observed. Repeatability of the testing procedure was demonstrated by repeating selected cases three times. Coefficients of variation from 3-20% were observed in these cases, demonstrating the repeatability of the procedure.

To determine the 1% and 5% separation times from the experimental data, first a linear least squares fit of the initial linear portion of the experimentally measured surface temperatures over the center of the defect was made. This establishes the "early time" slope (ET slope). This slope is used along with Equation 1[6] to determine the applied heat flux during the test to use it in the finite element models. If the initial slope did not intersect the time axis at the origin (due to variations between the times when the shutters were removed from the heat sources and the camera was activated), the time axis was shifted to define time equal zero at the onset of temperature rise. The experimental data were then fit to a 4^{th} order polynomial using the least squares method (to minimize the effect of signal noise on the following step). Intersection between the polynomial curve fit and a line with a slope of 1.01x the early time slope was used to determine the separation time according to the 1% deviation criterion. The 5% separation time was determined similarly. The 1% and 5% separation times of the resistive defects specimens determined by this process are listed in Table 4. Table 4 also shows the predicted defect depth from 1% and 5% deviation based on the one-dimensional infinite resistance solution, Equation 6. The results show significant errors, especially for the lower thermal resistance defects due to the heat transfer through the defects. These errors could be reduced by correcting Equation 6 for known finite

resistance ratio, which can be computed based on the geometry of these defects, as described in Section 3.2. For actual defects, however, the resistance ratio is not known in advance. The two-point method described in Section 3.3, however, allows both the defect resistance and its depth to be simultaneously obtained and thus provides a more general procedure for application to actual defects in structures with unknown defects.

The two-point method was applied to results of this experimental study, and results are tabulated in Table 4. Except for the lowest resistance ratio case, the defect depth measurements are excellent, with errors less than 3%. Resistance ratio is less accurately predicted, but with the exception of the outlier case, all errors are less than 20%. More detailed error analysis is under review.

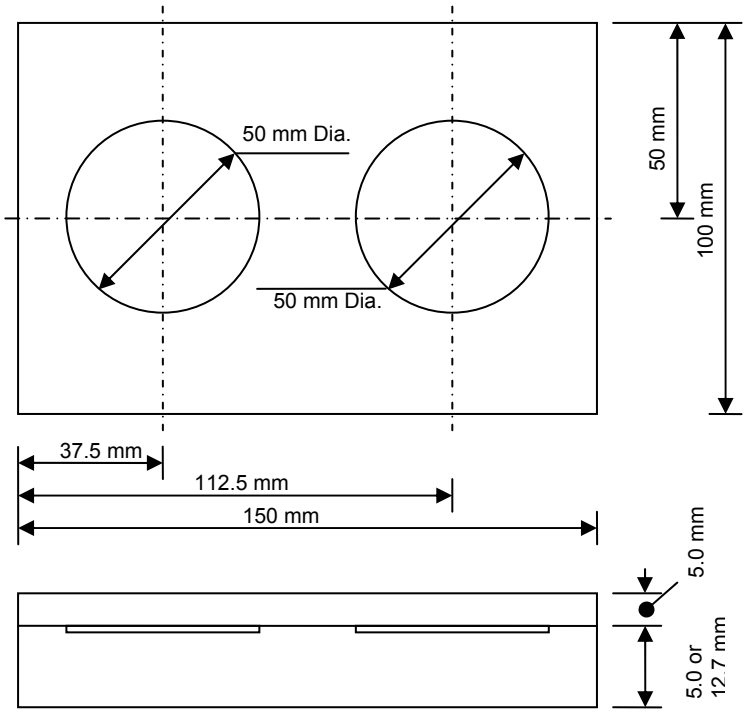

Figure 8. Sketch of a sample with a disk shaped inclusion.

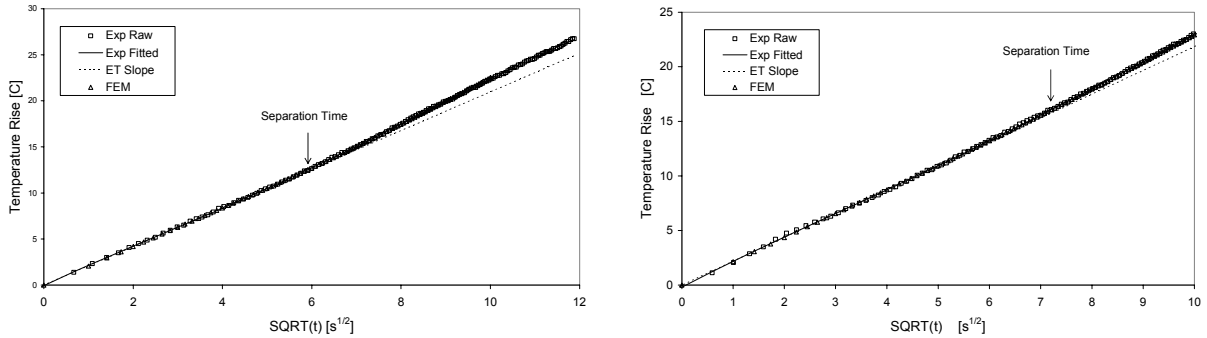

(a) (b)

Figure 9. Experimental and simulation of the temperature rise over the center of defects: (a) 160 μm thickness defect located at 5.0 mm depth in 17.7 mm thick GFRP structure, (b) 86 μm thickness defect located at 5.0 mm depth in a 10.0 mm thick GFRP structure.

Table 4. Comparison between the defect depth prediction based on the infinite resistance solution and resistive solution using the two point method. All defects are at 5.0 mm depth.

Actual			Experimental		Infinite Resistance Solution		Resistive Solution using two-point method			
Defect Thick. (μm)	Sample Thick. (mm)	Resist. Ratio	1% Separation Time (s)	5% Separation Time (s)	Predicted Depth (mm)	Error (%)	Resist. Ratio	Error (%)	Predicted Depth (mm)	Error (%)
38	10.0	0.1695	52.9	116.4	7.23	44.6	0.6126	261.4	6.12	22.4
65	10.0	0.2900	42.6	117.1	6.89	37.8	0.3363	16.0	5.14	2.8
86	10.0	0.3833	38.8	103.4	6.52	30.4	0.3604	-6.0	4.95	-1.0
282	10.0	1.2582	31.6	60.2	5.38	7.6	1.1892	-5.5	4.93	-1.4
160	17.7	0.7138	35.0	75.2	5.84	16.8	0.6727	-5.8	5.02	0.4
205	17.7	0.9150	34.0	70.7	5.71	14.2	0.7447	-18.6	4.98	-0.4
230	17.7	1.0260	32.7	65.6	5.55	11.0	0.8889	-13.4	4.94	-1.2
300	17.7	1.3385	32.6	61.2	5.44	8.8	1.3453	0.5	5.04	0.8

6. CONCLUSIONS

Techniques for identifying defects in thick composite using step heating thermography have been investigated. An analytical one-dimensional solution has been used to investigate the problem, and limitations of the model have been identified using finite element analysis. A simple two-point correlation method has been developed to simultaneously predict the defect depth and thermal resistance of defects from the early time behavior of the surface temperatures over the defects. The method is demonstrated using finite element results and experimental tests of samples containing embedded void defects. Good agreement is obtained in most cases using the two-point method. Key conclusions are as follows:

- Defect depth prediction using correlation with infinite resistance solutions produces substantial errors, even for defects with moderately large thermal resistance.
- The two-point method allows accurate determination of defect depth across a range of test geometries.
- Determination of defect thermal resistance using the two-point method is less accurate than defect depth.
- Accuracy of measurements of both defect depth and resistance appear to be functions of defect depth.
- Finite element models suggest that accurate measurements are possible for defect geometries with diameter to depth ratios of four or greater for the present methods based on effective contrast of up to 5%.

Accurate results have not been demonstrated for very low resistance defects, such as would coincide with simple closed delaminations. For accurate prediction of very thin delaminations, the defects need to be close to the front surface. Future research will concentrate on the field implementation of the proposed procedure to quantitatively predict the defects in composite pipes used in the petroleum industry.

ACKNOWLEDGEMENTS

Equipment used in this work was provided by the Saudi Arabia Oil Company (Saudi Aramco). The authors would like to thank Mr. William Bailey and Mr. John Lee for their help in preparing test specimens.

REFERENCES

1. D. Maillet, A. Houlbert, S. Didierjean, A. Lamine, and A. Degiovanni, “Non-destructive thermal evaluation of delamination in a laminate: Part I- Identification by measurement of thermal contrast,” Composites Science and Technology **47**, 137-153 (1993).
2. W. P. Winfree and J. N. Zalameda, “Thermographic determination of delamination depth in composites,” in Thermosense XXV, K.E. Cramer and X.P. Maldague, eds. Proc. SPIE **5073**, 363-373 (2003).

3. R. Gupta, and S. Tuli, "Electrical approach to defect depth estimation by stepped infrared thermography" IEE Proc.-Sci. Meas. Technol. **151(4)**, 298-304 (2004).
4. J. G. Sun, "Analysis of pulsed thermography methods for defect depth prediction," Journal of Heat Transfer, **128**, 329-338 (2006).
5. X. P. Maldauge, *Theory and practice of infrared technology for nondestructive testing*, John Wiley & Sons, Inc., New York, 2001.
6. H. S. Carslaw and J. C. Jeager, *Conduction of heat in solids*, Oxford University Press, London, 1959.
7. L. Brancik, "Programs for fast numerical inversion of Laplace transforms in MATLAB language environment," Sbornik 7. Proc. MATLAB 99, Prague, 27-39 (1999).
8. A. A. Badghaish and D. C. Fleming, "Nondestructive inspection of composite using step heating thermography," Proceedings of the American Society of Composites 22nd Technical Conference, Sept. 17-19, 2007, Seattle, WA, (2007).
9. L. Favro, X. Han, P. Kuo, and R. Thomas. "Imaging the early time behavior of reflected thermal-wave pulses," in Thermosense XVII, S. A. Semanovich, ed. Proc. SPIE **2473**, 162-166 (1995).
10. S. K. Lau, D. P. Almond, and J. M. Milne. "A quantitative analysis of pulsed video thermography," NDT&E International, **22 (4)** 195-202 (1991).
11. Anon. McMaster-Carr Supply Co. Doc. 8549KAC (2007).